3D printed systems for colon-specific delivery of camptothecin-loaded chitosan micelles

Andreia Almeida[a, b, c, †], Vicente Linares[d, †], Gloria Mora-Castaño[d], Marta Casas[d], Isidoro Caraballo[d], Bruno Sarmento[a, b, e*]

[a] INEB - Instituto Nacional de Engenharia Biomédica, Universidade do Porto, Rua Alfredo Allen, 208, 4200-135, Porto, Portugal

[b] i3S – Instituto de Investigação e Inovação em Saúde, Universidade do Porto, Rua Alfredo Allen, 208, 4200-135, Porto, Portugal

[c] Instituto de Ciências Biomédicas Abel Salazar, Universidade do Porto, Rua Jorge Viterbo Ferreira, 228, 4050-313, Porto, Portugal

[d] Department of Pharmacy and Pharmaceutical Technology, Faculty of Pharmacy, Universidad de Sevilla, C/Profesor García González 2, 41012 Seville, Spain.

[e] CESPU, Instituto de Investigação e Formação Avançada em Ciências e Tecnologias da Saúde, Rua Central da Gandra, 137, 4585-116, Gandra, Portugal

[†] Equal contribution

*Corresponding author: Tel +351 226074949, bruno.sarmento@i3s.up.pt

Abstract: The use of 3D printing technology in the manufacturing of drug delivery systems has expanded and benefit of a customized care. The ability to create tailor-made structures filled with drugs/delivery systems with suitable drug dosage is especially appealing in the field of nanomedicine. In this work, chitosan-based polymeric micelles loaded with camptothecin (CPT) were incorporated into 3D printing systems (printfills) sealed with an enteric layer, aiming to protect the nanosystems from the harsh environment of the gastrointestinal tract (GIT). Polymeric micelles and printfills were fully characterized and, a simulated digestion of the 3D systems upon an oral administration was performed. The printfills maintained intact at the simulated gastric pH of the stomach and, only released the micelles at the colonic pH. From there, the dissolution media was used to recreate the intestinal absorption and, chitosan micelles showed a significant increase of the CPT permeability compared to the free drug, reaching

an apparent permeability coefficient (P_{app}) of around 9×10^{-6} cm/s in a 3D intestinal cell-based model. The combination of 3D printing with nanotechnology appears to have great potential for the colon-specific release of polymeric micelles, thereby increasing intestinal absorption while protecting the system/drug from degradation throughout the GIT.

Keywords: 3D printing; polymeric micelles; oral administration; colon-specific delivery; intestinal permeability.

1. Introduction

The oral route is the most preferred via of administration of drugs due to the greatest patient compliance and ease of administration. In the market, drugs for oral administration are the most used worldwide, however, some drugs present poor oral availability and cannot be administered orally. This is the case of several anticancer drugs, that despite being effective against cancer, cannot be administered orally due to the poor aqueous solubility and low intestinal permeability [1, 2].

Camptothecin (CPT) was found in the bark of the Chinese tree, *Camptotheca acuminate* [3] and, is a potent anticancer drug against several types of cancer, including colorectal cancer. Its mechanism of action is based on the inhibition of the nuclear DNA topoisomerase I (TOP1) by binding the complex DNA-TOP1, leading to DNA damage and, subsequently, to cell apoptosis [4]. CPT belongs to the Class IV of the Biopharmaceutical Classification System (BCS), which means to have low solubility and low permeability. Indeed, CPT present some toxicity, its physical-chemical stability is pH dependent and can suffer hydrolysis if administered orally due to the chemical and enzymatical barriers of the gastrointestinal tract (GIT). Additionally, the poor oral bioavailability is a result of the high level of the first pass metabolism and the action of drug efflux transporters, as the P-glycoproteins (P-gp) [5]. Thus, there is a great need to overcome these drawbacks in order to be able to deliver CPT efficiently after an oral administration.

Nanotechnology has changed the field of drug delivery and, particular attention has been given to oral administration of drugs [6-8]. Polymeric micelles are nanosystems constituted by a hydrophobic core and a hydrophilic shell widely

used in the encapsulation of hydrophobic drugs. These systems are described as potential oral vehicle of delivery since they can protect the drug from the harsh environment of the GIT, increasing its stability. Polymeric micelles are attractive also due to the high drug encapsulation capacity, where a therapeutic dose can be reached easily, avoiding side-effects and avoid efflux pumps of the epithelium [9-11].

Chitosan is a natural polymer extensively used in the production of polymeric micelles due to the ease of modification into an amphiphilic polymer with self-assembly properties. Moreover, chitosan has mucoadhesive properties and has the ability to temporarily open the tight junctions of the epithelium, properties that can enhance the intestinal permeability of drugs [12].

Three-dimensional printing (3DP) is gaining interest in pharmaceuticals by virtue of its ability to manufacture medicines with freeform geometries and flexibility in dose, drug release, etc. Thanks to its versatility, 3DP for medicines has become an interesting tool for drug personalization specially for paediatric and geriatric population due to their particular physiological needs [13-16].

Several 3DP techniques have been successfully employed for medicine manufacturing. Between them, fused deposition modelling (FDM) is one of the most common for its easy use, acceptable level of accuracy and good reproducibility. However, one of the main drawbacks is the impossibility to print thermolabile drugs due to the high temperatures achieved both during the drug loading process of the thermoplastic filament, and the 3D printing process [17]. Consequently, for thermo-sensitive pharmaceutical formulations, FDM does not appear to be the best option. Nevertheless, we have already shown the potential of combining two 3DP techniques (FDM and injection volume filling (IVF)) in one bioprinter to overcome this limitation [18]. IVF is based on a syringes system which works with low pressure injections, being useful for dispersions, suspensions, and low-viscosity pastes. As a result, 3D printed systems filled with a liquid or semisolid pharmaceutical formulation, called printfills, were developed. Thanks to the combination of FDM and IVF, the drug and a pH-sensitive polymer were incorporated in the scaffold produced by FDM at once, in a continuous and automated process.

Targeted drug delivery together with dose personalization can improve the patient´s standard of living [19, 20]. Therefore, the ease to design modified drug

release systems is a valuable advantage of 3DP for medicines. In this sense, colonic drug release becomes a potential area for 3DP, especially for the treatment of colonic diseases like Crohn disease, cancer, or ulcers [21, 22].

The aim of this study was to protect chitosan-based micelles loading CPT from the harsh environment of the GIT, allowing the release of micelles in the colon, improving the intestinal permeability of CPT. Free CPT and loaded into micelles [23] were incorporated in printfills manufactured through an automated manufacturing 3D printing process.

2. Materials and methods

2.1. Materials

Polylactic acid (PLA) was chosen as biodegradable thermoplastic filament for FDM (grade Ingeo 3D850, peak melt temperature 165-180ºC, melting point 220ºC, density 1.25 g/cm^3), supplied by Leon3D (Spain). Eudragit FS30D (Evonik, Germany) was employed as delayed release polymer. CPT was purchased from Hangzhou ROYAL Import & Export Co., Ltd; 3.5 kDa cutoff dialysis membrane (regenerated cellulose, Spectra/Por® 3 Dialysis Tubing, Fisher Scientific) was used to produce the micelles.

2.2. Methods

2.2.1. Production of camptothecin-loaded polymeric micelles

Polymeric micelles based on chitosan were obtained by a dialysis method, as previously described [23, 24], however, the CPT association efficiency (AE) was optimized and improved from the last published work [23]. Briefly, 10 mg of *O*-methyl-*O′*-succinylpolyethylene glycol-chitosan-oleic acid (mPEG-CS-OA polymer) were dissolved in 4 mL of dimethyl sulfoxide (DMSO):HCl 0.1 M (9:1) in a glass tube and left overnight at RT until its complete dissolution. CPT, previously dissolved in DMSO at 1 mg/mL, was added to the prior solution at different drug loadings (w/w). The mixture continued under stirring and, after 6 h, dialyzed with three-cycle renewal against water to remove the DMSO and the non-associated CPT. Afterwards, CPT-loaded micelles were centrifuged during 20 min at 3110 g to remove the drug precipitate during dialysis, frozen with 0.5% (w/v) trehalose as a cryoprotectant, and freeze-dried to achieve the micellar powder.

2.2.2. Characterization of camptothecin-loaded micelles

Mean particle size, polydispersity index (PdI), and surface charge were assessed by dynamic light scattering (DLS) and Laser Doppler Micro-electrophoresis (ZetaSizer Nano ZS, Malvern, UK), respectively, with an angle of 173° at 25 °C. Polymeric micelles were analyzed freeze-drying resuspended in MilliQ water at 1% (w/v) concentration. Morphological analysis CPT-loaded mPEG-CS-OA micelles was assessed by transmission electron microscopy (TEM). Micelles were prepared on a grid treated with uranyl acetate and then examined in a JEM-1210 Transmission Electron Microscope (JEOL Ltd., Tokyo, Japan) operating at 120 kV. The AE was determined by the indirect method by high-performance liquid chromatography (HPLC) and calculated as described in Eq. (1). Drug loading (DL) was obtained according to Eq. (2). Briefly, the HPLC analysis was performed in a Shimadzu UFLC Prominence System (USA) equipped with two Pumps LC-20AD, a column oven CTO-20AC, an autosampler SIL-20AC, a System Controller CBM-20A, a degasser DGU- 20A5, a RF-10Axl fluorescence detector coupled to the LC System and a LC Solution, Version 1.24 SP1 (Shimadzu), and the method used for CPT quantification was described by Martins *et al*., [25].

$$AE\% = \frac{weight\ of CPT\ added - weight\ of\ free\ CPT}{weight\ of\ CPT\ added} \times 100 \quad \text{Eq. (1)}$$

$$DL\% = \frac{weight\ of\ CPT\ added - weight\ of\ free\ CPT}{total\ micelles\ weight} \times 100 \quad \text{Eq. (2)}$$

2.2.3. 3D printed systems production

Printfills (3D printed systems) were manufactured employing a bioprinter (Regemat 3D S.L., Spain) which combines FDM and IVF techniques. Two different batches of printfills were designed by the software Regemat 3D DESIGNER. First batch contained free CPT, whereas the second one CPT encapsulated within polymeric micelles.

2.2.3.1 Preparation of drug printable ink

Suitable drug printable inks were prepared for each batch: Firstly, free CPT dissolved in DMSO with a concentration of 5 mg/mL was diluted in a dissolution

of 10 mL DMSO:dH_2O at a ratio of 7:3. Secondly, to obtain printable ink with lyophilized CPT loaded-micelles, 4.5 mL of dH_2O were employed to rehydrate and resuspend the micelles. Both printable inks were prepared with the minimum light exposure to reduce the interaction with the drug.

2.2.3.2. 3D printing process

Printing settings for each batch are shown in Tables S1 and S2 in the supplementary materials. Due to the different composition of the two drug inks, systems prepared with micelles required more injection points and lower deposit speed in order to ensure the same volume incorporated in the structure. Also, the amount of Eudragit FS30D was higher to ensure the top face sealing of the printfill (Table S1 and Table S2).

According to the digital design of the 3D printed system, printfills were built layer by layer (Figure S1). FDM starts the printing process building the scaffold in the platform by extruding 2 bottom solid layers. The extrusion continues with parallels lines separated by 1.8 mm and 2 mm for free CPT batches and CPT encapsulated, respectively. The next layer is built with perpendicular lines respect to the lower one, resulting in a quadrilateral mesh of 1.8×1.8 mm and 2×2 mm for each batch. This process continues until the18th layer of the scaffold when the two automated syringes of IVF inject inside the scaffold. The first syringe contained printable ink with the free CPT and injected 200 µL in the 18th layer in 4 different points of the mesh, whereas 12 injection points were necessary for micelles. Again, FDM continues extruding a couple of layers to finish the scaffolds. Finally, IVF with the second syringe injected the set volume of the delaying polymer in the last layer of the system sealing the top face of the printfill. All 3DP process from the FDM extrusion until the last injection of IVF was a continuous and automatic manufacturing. Once the printfills were finished, were dried in a drying oven (632 plus Nahita, Auxilab S.L., Navarra, Spain) at 29 ºC for 24 h to evaporate the solvent (Figure S2 in the supplementary materials).

2.2.4. Characterization of the 3D printed systems

2.2.4.1. Physical characteristics of 3D printed systems

Printfills were weighed in a precision balance (Scaltec, type SBC31) and thickness and diameter were measured using a digital micrometer (Comecta, SA).

2.2.4.2. Scanning electron microscopy (SEM)

The interior mesh and transversal section of the delaying polymer were evaluated in the Microscopy Service of the CITIUS in the University of Seville by using scanning electron microscopy (SEM) with a FEI TENEO electronic microscope (FEI Company, USA), operating at 5 kV. Printfills were coated with a 12 nm thin Pt/Pd layer with Leica EM SCD500 high vacuum sputter coater.

2.2.5. Camptothecin release from the printfills

The dissolution studies were carried out using a USP Apparatus I Sotax AT7 smart (Allschwil, Switzerland) at 37 ± 0.5 °C with a rotation speed of 50 rpm. Printfills were exposed to different switch solutions (SS) to mimic the intestinal transit according to Schellekens *et al*., [26]. Their methodology was modified to prolong the colon residence time, as shown in Table S3 in the supplementary materials. The different SS (Table S4 in the supplementary materials) were added from one phase to another to obtain the required pH. Samples were withdrawn at specific interval times: 1, 2, 2.5, 3.5, 4.0, 4.2, 4.3, 4.5, 4.8, 5.0, 5.3, 5.5, 6.0, 6.5, 7.0, 7.5, 8 hours. The amount of CPT released from the printfills at each time-point was quantified by HPLC, as previously described [25]. The results are present as a cumulative percentage of CPT released at each analyzed time (*n=6*). Drug release data ($M_t/M_\infty \leq 0.8$) was also analysed using Microsoft Excel 2010 (Microsoft, Albuquerque, NM, USA) according to zero order, Higuchi [27], Korsmeyer *et al*., [28] and Peppas and Sahlin [29], following the Equations (3) – (5):

$$\frac{M_t}{M_\infty} = bt^{1/2} \quad \text{Eq. (3)}$$

$$\frac{M_t}{M_\infty} = k_k t^n \quad \text{Eq. (4)}$$

$$\frac{M_t}{M_\infty} = k_d t^m + k_r t^{2m} \quad \text{Eq. (5)}$$

where M_t/M_∞ is the drug released fraction at time *t* (the drug loading was considered as M_∞), *b* and k_k are kinetic constants characteristic of the drug/polymer system, *t* is the release time, *n* is the release exponent that depends on the release mechanism and the shape of the matrix tested, k_d and k_r are the diffusion and relaxation rate constants, respectively, *m* is the purely Fickian diffusion exponent for a device of any geometrical shape which exhibits controlled release. Determination coefficient (r_2) was used to test the applicability of the release models, calculated in linear regression for zero order, Higuchi and Korsmeyer equations or quadratic regression for Peppas and Sahlin model.

2.2.6. Cell culture

C2BBe1 [Caco-2 clone] (human colorectal adenocarcinoma) cells were acquired from ATCC and HT29-MTX mucus-producing cells were kindly provided by Dr. T. Lesuffleur (INSERM U178, Villejuif, France). Both cell lines were maintained in complete medium comprising Dulbecco's Modified Eagle's Medium (DMEM, ATCC) supplemented with 10% (v/v) Fetal Bovine Serum (FBS, Biochrom) and 1% (v/v) antibiotic-antimitotic mixture (final concentration of 100 U/mL penicillin and 100 U/mL streptomycin, Biowest). Human intestinal fibroblast (HIF) primary cells were obtained from ScienCell and maintained in culture with Fibroblast Medium (FM) supplemented with 2% FBS, 1% of Fibroblast Growth Supplement (FGS), and 1% penicillin/streptomycin solution (all supplements from ScienCell). HPMEC-St1.6R cells were kindly provided by Professor C. James Kirkpatrick (Institute of Pathology, Johannes Gutenberg University of Mainz, Germany) and were maintained with M199 medium (Sigma), supplemented with 20% FBS (Biochrom), 1% (v/v) antibiotic-antimitotic mixture (final concentration of 100 U/mL penicillin and 100 U/mL streptomycin, Biowest), 25 µg/mL of Endothelial Cell Growth Supplement (ECGS) and 25 µg/mL of heparin (both from Sigma), and 100 µg/mL L-glutamine (LabClinics). All the cells were cultures in 75 cm^2 T-flasks, inside an incubator at 37 ºC and 5% CO_2 and 95% relative humidity.

2.2.7. Metabolic assay using drug and micelle released medium

To assess the safety of the micelles and the free drug to be placed in the permeability assay, the released media from the printfills of the CPT and CPT-loaded micelles was used to perform a resazurin assay. Briefly, 2×10^4 Caco-2

cells were seeded in 96-well plates and incubated at 37 ºC and 5% CO_2 and 95% relative humidity during 24 h to allow the cells to adhere to the wells. Then, the medium was removed and cells were washed twice with pre-warmed PBS and, treated with 200 µL of the release media from the printfills of the free CPT and CPT-loaded micelles diluted 1:1 with DMEM complete medium and, allowed to incubate for 4, 6 and 24 h. After that, the medium was removed and cells were washed twice with pre-warmed PBS and incubated with DMEM complete medium with 20% resazurin (0.1 mg/mL; Merck) during 2 h at 37 ºC, 5% CO_2 and 95% relative humidity, protected from the light, to allow viable cells reduce resazurin into the resorufin, which the pink and fluorescent product of the reaction. The fluorescence was measured by the relative fluorescence units (RFUs) by removing the supernatant of the previous plate into black 96-well plates using a microplate reader SynergyTM Mx HM550 (Biotek) set at 530/590 (excitation/emission wavelength, respectively). A negative control consisting in cells incubated with 1% (v/v) of Triton X-100 in complete medium and a positive control consisting in cells incubated with complete medium were also included in the experiment. A number of six replicates were performed for each group and, the metabolic activity was quantified according to Eq. 6:

$$Cellular\ viability\ (\%) = \frac{fluorescence\ (experimental\ value) - fluorescence\ (positive\ control)}{fluorescence\ (negative\ control) - fluorescence\ (positive\ control)} \times 100 \quad \text{Eq. (6)}$$

2.2.8. Intestinal permeability models

Two different intestinal models were used to evaluate the intestinal permeability of CPT released from the printfills with free CPT and CPT-loaded micelles after passing through the simulated gastrointestinal fluids. The first one, constituted only by Caco-2 cells, which is the standard model to study the intestinal permeability of molecules; and the second one, constituted by Caco-2 cells, HT29-MTX mucus-producing cells, HIF embedded in a collagen coating and endothelial cells, a 3D model that better mimic what happens in an *in vivo* situation [30]. For the Caco-2 model, 1×10^5 cells per cm^2 were seeded in a 12-Transwell® cell culture inserts (pore size of 1 µm, Millicell) and allowed to grow and differentiate for 21 days inside an incubator at 37 ºC, 5% CO_2 and 95% relative humidity. The 3D intestinal model is similar to the previously published

work of our group [31], but it was improved for the presence of an endothelial layer mimicking the passage into the blood vessels [30]. Thus, in the 3D intestinal model, HPMEC-St1.6R cells were firstly seeded in a 0.2% gelatin coating in the basolateral side of the Transwell® insert at density of 5×10^4 cells/cm^2 and waited 2 h for the cells to adhere to the coating. After that, the inserts were placed in a 12-well plate and the apical side was coated with collagen with HIF embedded, which were incubated as previously described for 30 min. Then, 1×10^5 cells/cm^2 in a ratio of 9:1 (Caco-2:HT29-MTX) were seeded in the apical side of the inserts over the collagen coating. Both models used DMEM complete medium to culture the cells in the Transwell® inserts for 21 days, incubated as previously described and, the medium was changed every two/three days from the apical and basolateral sides. During 21 days, both models were monitored by the transepithelial electrical resistance (TEER) using an EVOM2 epithelial voltohmmeter equipped with a STX2 electrode (World Precision Instruments, Inc.), which gives the information about the integrity of the monolayer.

2.2.9. Camptothecin intestinal permeability

After 21 days the models sown, the medium was removed from both compartments and cells were washed twice with pre-warmed Hank's Balanced Salt Solution (HBSS) buffer and left to equilibrate with HBSS during 30 min at 37 ºC and 100 rpm in an orbital shaker (KS 4000 ic control orbital shaker, IKA). After 30 min, the HBSS was removed from the apical side and the released medium from the printfills from both free CPT and CPT-loaded micelles were added to the apical side of the insert (0.5 mL) and plates were again incubated at 37 ºC and 100 rpm. At predetermined time points (15, 30, 60, 180, and 240 min), a 200 µL sample was taken from the basolateral side and the same volume of pre-warmed HBSS was added to the insert. The TEER was measured at each time-point in order to assess the monolayer integrity. The CPT permeated through the monolayers was quantified by HPLC, as previously described [25] and, the permeability percentage and apparent permeability coefficient (*Papp*) were determined through the Eq. 7 and Eq. 8, respectively.

$$CPT\ permeated\ \% = \frac{total\ mass}{theoretic\ mass} \times 100 \qquad \text{Eq. (7)}$$

$$Papp = \frac{dQ}{A \times C_0 \times dt}$$ Eq. (8)

where dQ (µg) is the total amount of compound in the basolateral side, A is the surface area of the insert (cm^2), C_0 is the initial concentration in the apical side (µg/mL) and *dt* (s) is the time of the experiment. The assay was performed in triplicate.

2.2.10. Cellular integrity by hematoxylin and eosin staining

To assess the integrity of the monolayers of the intestinal models after the permeability assay and, to ensure the permeability found was not due to the monolayer disruption, H&E staining was performed. Transwell® inserts were washed twice with PBS for 5 min and then fixed with 2% PFA in PBS during 20 min at RT. Then, the intestinal models were washed thrice with PBS during 5 min and kept at 4 ºC in PBS until further processing for paraffin embedding. Sections of 3 mm were collected using an RM2255 microtome (Leica) and then stained for H&E. Briefly, sections were deparaffinized and rehydrated, stained for 3 min in Gil's Hematoxylin (Thermo Scientific), 6 min in running water, dehydrated, stained for 1 min in Eosin Y (Thermo Scientific), cleared, and mounted in Entellan (Merck). Demonstrative images of each condition of the intestinal permeability were acquired with a Light microscope Olympus DP 25 Camera Software Cell B.

2.2.11. Statistical analysis

Statistical analysis was performed using the GraphPad Prism Software vs. 6.0 (GraphPad Software Inc). All data were presented as mean ± SD.

3. Results and discussion

3.1. Characterization of camptothecin-loaded micelles

In this study, CPT was associated to chitosan micelles by dialysis method and characterized by the average size, PdI and surface charge. The AE and DL was also calculated, where the last was optimized from our last work [23]. As can be seen from Table 1, empty micelles presented an average size of around 130 nm and, as the CPT was physical entrapped to the system with the DL increasing, the average size of the micelles also increased. This expansion volume of the

micelles can be due to the accumulation of large amounts of hydrophobic groups on the micelle core, which means the CPT encapsulation have a direct influence on micelle average size. At the same time, the PdI also increased with DL increasing. Taking into consideration the data found in the literature, systems with PdI values below 0.3 represent monodispersed systems [32, 33]. Therefore, the formulation with 20% (w/w) CPT did not represent a monodispersed distribution and, thus, should not proceed for the further studies. The high PdI is typical found on chitosan-based micelles due to the heterogeneity of the polymer and the non-uniform distribution of the acyl chains on the chitosan backbone as result of the reaction with the substituent groups to obtain new chitosan derivatives. Nevertheless, the values found are in agreement with the literature for other chitosan derivatives [34, 35].

The micelles surface charge also presented a direct influence with the DL increasing. As CPT is entrapped into the mPEG-CS-OA micelles, their surface charge changed from +37 mV to +44 mV (Table 1). This comportment may be explained by the fact that micelles were formed by the interaction of the hydrophobic moieties of the polymer chain with the hydrophobic segments of the drug. Thus, with the DL increasing, the hydrophobic moieties also increased, leading to a higher exposure of the hydrophilic segments of chitosan, which is positively charged. The fact the micelles presented a highly positive surface charge may favor the interaction with epithelial cells, leading to a higher CPT absorption.

Regarding the AE of mPEG-CS-OA micelles, it was verified a decreased AE with the DL_T increasing, due to the saturation of the nanosystems. Indeed, despite the decrease on the AE, the DL of the micelles increased, as previously observed [36, 37]. The formulation with 20% (w/w), despite having around 1% more drug, showed more polydispersity and a significantly larger diameter than the other formulations. Thus, the formulation of mPEG-CS-OA micelles with 15% (w/w) DL_T was chosen for further experiments due to the demonstrated monodispersed character together with a high amount of CPT associated into the micelles.

Table 1 - The theoretical drug loading (DL_T), association efficiency (AE), the drug loading (DL), particle size, PdI and micelles surface charge empty and CPT-loaded mPEG-CS-OA micelles. Values are represented as mean ± SD (n = 3).

DL_T (%)	AE (%)	DL (%)	Size (nm)	PdI	Zeta potential (mV)
0	-	-	132 ± 3	0.262 ± 0.026	37.5 ± 0.2
5	78.4 ± 2.2	3.9 ± 0.1	155 ± 15	0.272 ± 0.033	41.3 ± 2.8
10	62.7 ± 5.5	6.3 ± 0.5	174 ± 26	0.286 ± 0.015	42.3 ± 3.6
15	55.5 ± 8.9	8.3 ± 1.3	178 ± 6	0.281 ± 0.016	42.8 ± 4.3
20	45.4 ± 2.9	9.1 ± 0.6	262 ± 25	0.324 ± 0.021	43.9 ± 3.3

3.2. Characterization of the 3D printed systems

3.2.1 Physical characteristics of 3D printed systems

Table 2 and 3 show the weights and dimensions of printfills according to the digital design. As expected, FDM technology worked with accuracy and precision during 3DP systems manufacturing. The dimensions of the printfills are susceptible of being modified according to the drug formulation and the dose. In addition, 3DP design can be modified in order to change the space available in the scaffold leading a smaller system.

Table 2 – Physical characteristics of printfills with free CPT and CPT-loaded micelles (n=6).

	Experimental			Theoretical	
Printfill with free CPT	**Weight (mg)**	**Height (mm)**	**Diameter (mm)**	**Height (mm)**	**Diameter (mm)**
Mean	1523.85	7.403	14.867	7.35	14
SD	79.116	0.204	0.053	0.038[a]	0.613[a]
CV	5.1918	2.758	0.358	0.513[a]	4.381[a]
Printfill with CPT-loaded micelles	**Weight (mg)**	**Height (mm)**	**Diameter (mm)**	**Height (mm)**	**Diameter (mm)**
Mean	1364.0	7.643	14.811	7.35	14
SD	63.746	0.250	0.080	0.207[a]	0.574[a]
CV	4.6736	3.266	0.538	2.820[a]	4.098[a]

[a] Calculated between theoretical and mean of experimental data.

3.2.2 Scanning electron microscopy (SEM)

SEM images depict the internal structure of printfills (Figure 1). The cross section of the 3DP system reveals a homogenous film of Eudragit FS30D at the top

confirming a sealing layer with a thickness of about 50 µm in the narrowest part. (Figure 1, A). Furthermore, evidence of the perimeter sealing of the scaffold can be found on supplementary material (Figure S3). Thus, the only water inlet available is through the upper face of the printfill, once the delaying polymer is dissolved at enteric pH. SEM cross section images of printfills with free drug showed recrystallized CPT on PLA after the drying process (Figure 1, B). Although printing settings were modified in order to inject the printable ink reducing the interaction between both delaying polymer and micelles, part of the printable ink remained embedded in the polymer after the drying process. Soaked micelles in the polymer Eudragit FS 30D can be seen in Figure 1 C and D.

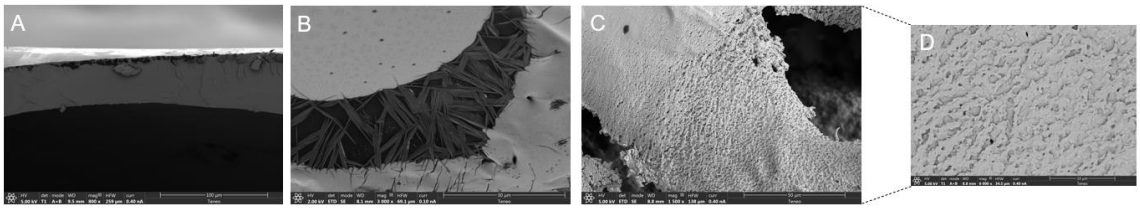

Figure 1 – Scanning electron microscopy images of (A) Eudragit top layer of the printfill; (B) CPT crystals inside of the printfill; (C) CPT-loaded micelles inside of the printfill; (D) amplification of the printfill with polymeric micelles inside. Scale bar corresponding to 100, 30, 50 and 10 µm, respectively.

3.3. *In vitro* release profile of camptothecin from the printfills loaded with polymeric micelles

As can be seen in the Figure 2, printfills with free drug and micelles were able to control the drug release. Thus, there was no drug released from the printfills during 2 h in pH 1.2. Once SS was added changing the pH to 6.8, the delaying polymer started to dissolve allowing the entrance of the water.

Printfills with free drug released 70% of CPT in less than 30 minutes at pH 6.8. The total amount of CPT obtained for this batch confirms the precision of IVF technology injecting the printable ink. On the other hand, printfills with CPT-loaded micelles showed a slower drug release (approximately 3%) due to the drug encapsulation within the polymeric micelles. Furthermore, it was evident the shape changes of release profiles, showing the micelles a sigmoid profile, typically of erosive systems.

Drug release data ($M_t/M_\infty < 0.8$) from printfills with CPT-loaded micelles were analyzed according to zero order, Higuchi, Korsmeyer–Peppas and, Peppas and Sahlin equations (Table 3). In the case of printfills with free CPT, the fast drug release did not allow to perform this study. Determination coefficient values indicates a poor fit for the different kinetic models, that can be explained because drug release profile reaches an asymptote at around 35% w/w. Thus, in order to obtain information about drug release mechanism from this profile, data has been analyzed until 260 min, i.e., before reaching asymptote. In this case, the best fit corresponds to Peppas and Sahlin equation, with a clear prevalence of K_r over K_d. This indicates that the drug release mechanism was controlled mainly by erosion. The *n* value from Korsmeyer equation indicates a super case II transport, confirming that that the mechanism of drug release was erosion/relaxation controlled.

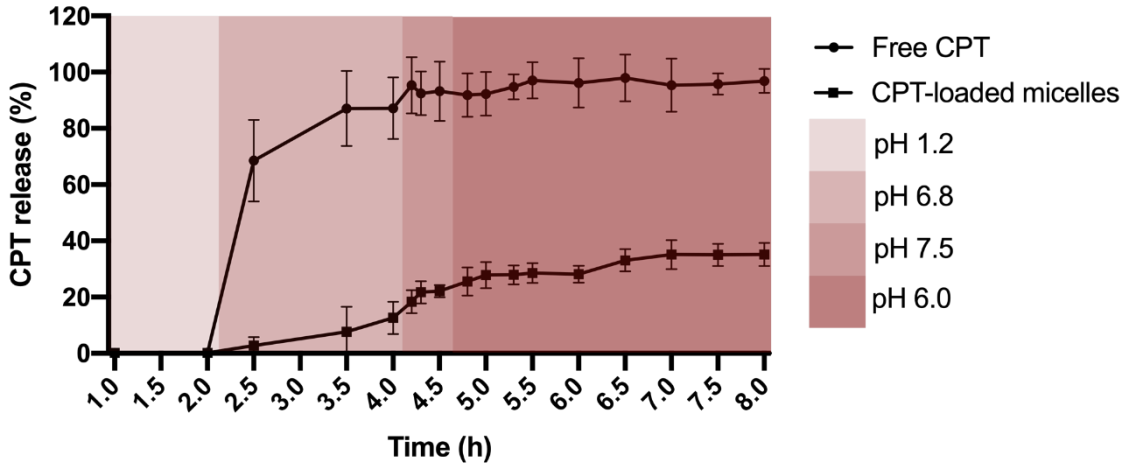

Figure 2 – Cumulative CPT release from the printfills in simulated gastrointestinal fluids. *Squares* represent the release of CPT-loaded micelles and *circles* represent the release of free CPT. Error bars represent mean ± SD (n = 6).

Table 3 – Mathematical modelling and drug release kinetics from the enteric printfills with CPT-loaded micelles up to 260 min.

Zero order	**Higuchi**		**Korsmeyer**			**Peppas and Sahlin**		
r^2	b ($min^{-0.5}$)	r^2	K_k (min^{-n})	n	r^2	K_d(min^{-m})	K_r(min^{-2m})	r^2
0.8586	0.0362	0.8995	$1.9113x10^{-6}$	2.0311	0.818	0.1245	-0.0025	0.9417

b, Higuchi kinetic constant; n, release exponent; k_k, Korsmeyer kinetic constant; k_d, Peppas diffusion kinetic constant; k_r, Peppas relaxation kinetic constant; r_2, determination coefficient.

3.4. *In vitro* cytocompatibility of polymeric micelles

In order to assess the safety and biocompatibility of the micelles and free CPT loaded in the printfills and released in the simulated gastrointestinal fluids (GIF), a resazurin assay was performed in Caco-2 cells during 4, 6 and 24 h of incubation. The micelles and free drug present in the dissolution medium after 6h were used to evaluate its cytotoxic potential. As we described before, the release of the micelles and drug only occurs at intestinal pH, thus, it only makes sense to evaluate safety by this way.

As can be seen in Figure 3, both polymeric micelles and free drug present in the dissolution media showed no cellular cytotoxicity against Caco-2 cells, a colorectal cancer cell line. Moreover, the metabolic activity of these cells increased up to 100%, which may be due to the presence of simulated GIF. Actually, according to the ISO 10993-5 guideline [38], it is reported that above 70% of cell viability is considered as safe, when testing *in vitro* formulations. Moreover, since we are working with a relatively low CPT concentration (< 10 µg) due to the slow CPT release and, based on previous published works [35, 39-41], it was expected no cytotoxic effect of the free CPT and CPT-loaded micelles present in the dissolution medium of the *in vitro* CPT release.

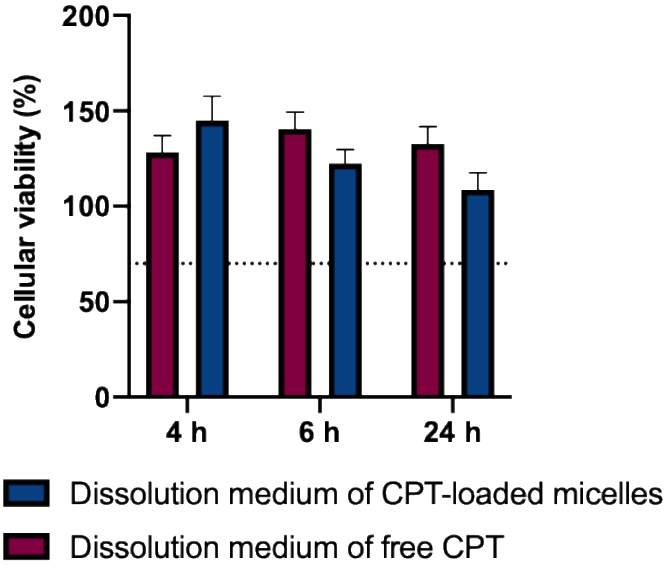

Figure 3 – Cellular viability of the dissolution medium from the printfills containing CPT-loaded micelles (blue columns) and free CPT (pink columns) after 4, 6 and 24 h of incubation with Caco-2 cells. Error bars represent mean ± SD (n = 6).

3.5. Permeability of camptothecin after simulated gastrointestinal passage

Printfills were prepared and filled with CPT-loaded micelles and free CPT. Then, they were placed in a simulated GIF to release both micelles and drug at the intestine to mimic oral intake. The dissolution medium at 6 h since the dissolution assay started was used to perform the permeability study.

To evaluate the CPT permeability, two different intestinal models were used, the 2D Caco-2 standard model and a 3D model, as previously described. As can be seen in Figure 4, the CPT permeability from the micelles was higher than the free drug in both models with significative differences at the last incubation times. The CPT permeability in the 3D model was around 27% which, compared to the standard model (20%), an enhanced intestinal permeability was verified. Since the 3D model represents the human intestine more closely, we are facing a drug permeability closer to the *in vivo* situation. Moreover, the P_{app} presented significative differences between micelles and free drug, where in the 3D model the P_{app} of CPT from the micelles reached values around 9×10^{-6} cm/s, which represents a great increase of the CPT permeability and bioavailability (Figure 4C). The free drug maintained the P_{app} around 5×10^{-6} cm/s in both models, which also describes the permeability of the free drug as being almost half of the permeability of the drug by the micelles, in the case of the 3D model. Silva *et al*., described CPT permeability of 4×10^{-6} cm/s and 8×10^{-6} cm/s for a similar system in a Caco-2 and a co-culture 2D model, respectively [35], which is very close to the results found in this work.

As it is widely known, chitosan has the ability to open the tight junctions of the epithelium [42]. In addition, chitosan has mucoadhesive properties and, in a more realistic model, as the 3D model, chitosan micelles can stick to the mucus layer and release the drug, also contributing to the CPT permeability enhancement and bioavailability. Indeed, other authors already described the interaction of chitosan with mucus layer, leading to a permeability increase [43, 44].

The TEER maintained stable during the experiment for both micelles and free drug, which is an indicative of the safety of the tested formulation [45]. The slight decrease observed after 1 h of the experiment starting may be related to the permeability increase, possible due to the opening of the tight junctions of the epithelium [46], which then increasing again in the end in the experiment.

Overall, chitosan micelles and free drug were maintained stable after simulated oral administration and were protected within the printfills and only released at the intestinal pH, where the permeability was tested. Micelles significantly increased the CPT permeability in both models, especially in the 3D model, that better mimics what occurs *in vivo*. We are facing an increase in the bioavailability of CPT after an oral administration, which can be very useful for the treatment of various diseases, as the cancer therapy.

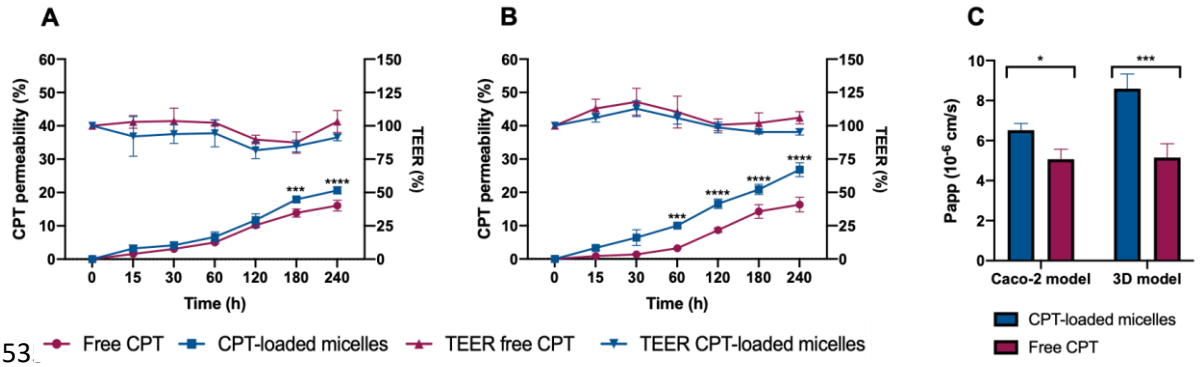

Figure 4 – Intestinal permeability and respective TEER values of the CPT-loaded micelles and free CPT after being released in the simulated GIF. (A) CPT permeability across Caco-2 standard model; (B) CPT permeability across a 3D intestinal model; (C) apparent permeability coefficients (P_{app}) of CPT-loaded micelles and free CPT across Caco-2 monoculture model and across the 3D model. All experiments were conducted from the apical to basolateral side in HBSS at 37 °C. Error bars represent mean ± SD (n = 3). *p<0.05, ***p<0.001 and ****p<0.0001 denotes a significant difference by two-way analysis of variance (ANOVA) Sidak's multiple comparison test.

3.6. Cellular integrity of the intestinal models

The TEER represents the integrity of the monolayer as previously mentioned, and thus, TEER values during 21 days of culture can be seen in the supplementary material (Figure S4). This can guarantee that the monolayer was formed and ready for the permeability studies. Also, during the permeability assay, the TEER was registered and, as described above, the values were maintained at the end of the experiment, meaning the permeability obtained was not due to the monolayer disruption. Moreover, to ensure the integrity of the membrane after the permeability experiment, hematoxylin and eosin (H&E) staining was performed for both models and conditions (Figure 6). For this assay, two dyes were used, hematoxylin and eosin, which are basic and acidic dyes,

respectively. Hematoxylin stains acidic structures in purple, as the nucleus and, eosin dyes basic structures in pink, as the cytoplasm and extracellular matrix [47]. Taking this into account, in Figure 6 is possible to observe a continuous monolayer in both models, corroborating with the TEER values, i. e., the cellular membrane integrity was maintained. Also, it is possible to visualize some portions of the monolayer where the membrane suffered disruption, but it was due to the handling procedure, which happens sometimes. In the case of the 3D model, it is possible to see a collagen layer with fibroblast embedded, as described in the methods section. Absence of cytotoxicity of chitosan-based micelles was also demonstrated by others authors [48-50]. Overall, the TEER values and the H&E staining support the hypothesis that the increased permeability is not due to the membrane disruption because, as demonstrated, it remains intact and tightly formed during and after the permeability assay.

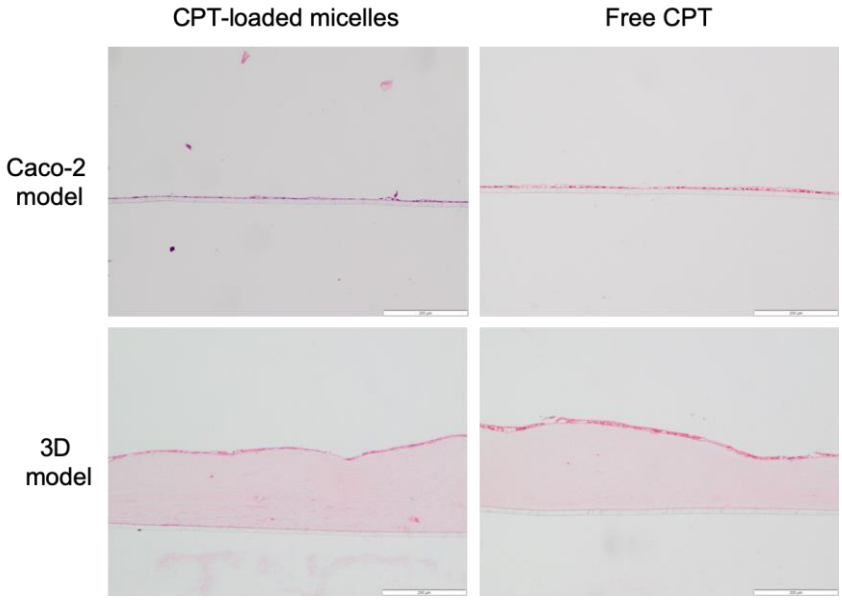

Figure 6 – H&E staining to address the cellular integrity when cells were exposed to the dissolution medium containing CPT-loaded micelles and free CPT for the permeability assay. Cytoplasm stained with pink and nucleus with purple. The Transwell® membrane is transparent and is right below the cellular monolayer. Scale bar = 100 µm.

Conclusion

Chitosan-based micelles loaded with CPT presenting an average diameter <200 nm were efficiently filled into 3D systems covered by an enteric layer. It was possible to verify the Eudragit top layer by SEM, as well as, the presence of the

polymeric micelles and free drug inside of the printfills. The dissolution assay demonstrated the printfills are able to maintain the micelles intact until they reach the intestinal pH. From the dissolution media mimicking a digestion upon oral administration of the printfills, it was possible to verify a significant increase of the intestinal permeability in both Caco-2 and 3D intestinal models. Thus, printfills filled with polymeric micelles were able to maintain them intact along the simulated gastrointestinal digestion and, specifically delivered it at the colonic pH. In this regard, it was possible to substantially increase the CPT intestinal absorption and, consequently, its oral availability avoid the enzymatic degradation and metabolization. This work showed a tremendous potential for a colonic-specific delivery of CPT-loaded micelles with proven improved intestinal absorption.

Acknowledgements

This article is based upon work from COST Action CA15216 “European Network of Bioadhesion Expertise: Fundamental Knowledge to Inspire Advanced Bonding Technologies” supported by COST (European Cooperation in Science and Technology) and by FCT - Fundação para a Ciência e a Tecnologia/ Ministério da Ciência, Tecnologia e Ensino Superior in the framework of the project “Institute for Research and Innovation in Health Sciences” (UID/BIM/04293/2019). Andreia Almeida (SFRH/BD/118721/2016) would like to thank to FCT, Portugal for financial support. The authors also acknowledge the support of the following i3S Scientific Platforms: Biointerfaces and Nanotechnology (FCT - UID/BIM/04293/2019) and Histology and Electron Microscopy (PPBI-POCI-01-0145-FEDER-022122). The authors would like to thank Ministerio de Ciencia, Innovación y Universidades of Spain (Grant RTI2018-095041-B-C31) for financial support.

Author Contributions

A.A. and **V.L.**, Conceptualization, Methodology, Writing - original draft; **M.C.**, Conceptualization, Methodology; **G.M.**, Conceptualization; **I.C.**, Conceptualization, Supervision, Writing - review & editing; **B.S.**, Conceptualization, Supervision, Writing - review & editing.

Declaration of Interest: none.

References

[1] L. Tu, G. Wang, N. Qi, W. Wu, W. Zhang, J. Feng, Multi-functional chitosan polymeric micelles as oral paclitaxel delivery systems for enhanced bioavailability and anti-tumor efficacy, Int. J. Pharm., 578 (2020) 119105.

[2] G. Qu, S. Hou, D. Qu, C. Tian, J. Zhu, L. Xue, C. Ju, C. Zhang, Self-assembled micelles based on N-octyl-N'-phthalyl-O-phosphoryl chitosan derivative as an effective oral carrier of paclitaxel, Carbohydr. Polym., 207 (2019) 428-439.

[3] M.E. Wall, M.C. Wani, Camptothecin and taxol: discovery to clinic—thirteenth Bruce F. Cain Memorial Award Lecture, Cancer Res., 55 (1995) 753-760.

[4] Y. Pommier, Topoisomerase I inhibitors: camptothecins and beyond, Nat. Rev. Cancer, 6 (2006) 789-802.

[5] Y. Xue, C. Ma, I. Hanna, G. Pan, Intestinal Transporter-Associated Drug Absorption and Toxicity, Adv. Exp. Med. Biol. , (2019) 361-405.

[6] G. Chen, D. Svirskis, W. Lu, M. Ying, Y. Huang, J. Wen, N-trimethyl chitosan nanoparticles and CSKSSDYQC peptide: N-trimethyl chitosan conjugates enhance the oral bioavailability of gemcitabine to treat breast cancer, J. Control. Release, 277 (2018) 142-153.

[7] R. He, C. Yin, Trimethyl chitosan based conjugates for oral and intravenous delivery of paclitaxel, Acta Biomater., 53 (2017) 355-366.

[8] R. Kumar, A. Sirvi, S. Kaur, S.K. Samal, S. Roy, A.T. Sangamwar, Polymeric micelles based on amphiphilic oleic acid modified carboxymethyl chitosan for oral drug delivery of bcs class iv compound: Intestinal permeability and pharmacokinetic evaluation, Eur. J. Pharm. Sci., 153 (2020) 105466.

[9] W.Y. Hu, Z.M. Wu, Q.Q. Yang, Y.J. Liu, J. Li, C.Y. Zhang, Smart pH-responsive polymeric micelles for programmed oral delivery of insulin, Colloids Surf. B, 183 (2019) 110443.

[10] X. Wang, Y. Guo, L. Qiu, X. Wang, T. Li, L. Han, H. Ouyang, W. Xu, K. Chu, Preparation and evaluation of carboxymethyl chitosan-rhein polymeric micelles with synergistic antitumor effect for oral delivery of paclitaxel, Carbohydr. Polym., 206 (2019) 121-131.

[11] C. He, Y. Jin, Y. Deng, Y. Zou, S. Han, C. Zhou, Y. Zhou, Y. Liu, Efficient oral delivery of poorly water-soluble drugs using carnitine/organic cation

transporter 2-mediated polymeric micelles, ACS Biomater. Sci. Eng. , 6 (2020) 2146-2158.
[12] R. Kumar, A. Sirvi, S. Kaur, S.K. Samal, S. Roy, A.T. Sangamwar, Polymeric micelles based on amphiphilic oleic acid modified carboxymethyl chitosan for oral drug delivery of bcs class iv compound: Intestinal permeability and pharmacokinetic evaluation, European Journal of Pharmaceutical Sciences, 153 (2020) 105466.
[13] Á. Aguilar-de-Leyva, V. Linares, M. Casas, I. Caraballo, 3D Printed Drug Delivery Systems Based on Natural Products, Pharmaceutics, 12 (2020) 620.
[14] C. Karavasili, A. Gkaragkounis, T. Moschakis, C. Ritzoulis, D.G. Fatouros, Pediatric-friendly chocolate-based dosage forms for the oral administration of both hydrophilic and lipophilic drugs fabricated with extrusion-based 3D printing, Eur. J. Pharm. Sci., 147 (2020) 105291.
[15] X. Xu, P. Robles-Martinez, C.M. Madla, F. Joubert, A. Goyanes, A.W. Basit, S. Gaisford, Stereolithography (SLA) 3D printing of an antihypertensive polyprintlet: Case study of an unexpected photopolymer-drug reaction, Addit. Manuf., 33 (2020) 101071.
[16] H. Herrada-Manchón, D. Rodríguez-González, M.A. Fernández, M. Suñé-Pou, P. Pérez-Lozano, E. García-Montoya, E. Aguilar, 3D printed gummies: Personalized drug dosage in a safe and appealing way, Int. J. Pharm., 587 (2020) 119687.
[17] G. Kollamaram, D.M. Croker, G.M. Walker, A. Goyanes, A.W. Basit, S. Gaisford, Low temperature fused deposition modeling (FDM) 3D printing of thermolabile drugs, Int. J. Pharm., 545 (2018) 144-152.
[18] V. Linares, M. Casas, I. Caraballo, Printfills: 3D printed systems combining fused deposition modeling and injection volume filling. Application to colon-specific drug delivery, Eur. J. Pharm. Biopharm., 134 (2019) 138-143.
[19] R. Govender, S. Abrahmsén-Alami, A. Larsson, S. Folestad, Therapy for the individual: Towards patient integration into the manufacturing and provision of pharmaceuticals, Eur. J. Pharm. Biopharm., 149 (2020) 58-76.
[20] T.C. Okwuosa, C. Soares, V. Gollwitzer, R. Habashy, P. Timmins, M.A. Alhnan, On demand manufacturing of patient-specific liquid capsules via co-ordinated 3D printing and liquid dispensing, Eur. J. Pharm. Sci., 118 (2018) 134-143.

[21] A. Goyanes, H. Chang, D. Sedough, G.B. Hatton, J. Wang, A. Buanz, S. Gaisford, A.W. Basit, Fabrication of controlled-release budesonide tablets via desktop (FDM) 3D printing, Int. J. Pharm., 496 (2015) 414-420.
[22] C.I. Gioumouxouzis, A.-T. Chatzitaki, C. Karavasili, O.L. Katsamenis, D. Tzetzis, E. Mystiridou, N. Bouropoulos, D.G. Fatouros, Controlled release of 5-fluorouracil from alginate beads encapsulated in 3D printed pH-responsive solid dosage forms, AAPS PharmSciTech, 19 (2018) 3362-3375.
[23] A. Almeida, M. Araújo, R. Novoa-Carballal, F. Andrade, H. Gonçalves, R.L. Reis, M. Lúcio, S. Schwartz, B. Sarmento, Novel amphiphilic chitosan micelles as carriers for hydrophobic anticancer drugs, Mater. Sci. Eng. C, 112 (2020) 110920.
[24] A. Almeida, D. Silva, V. Gonçalves, B. Sarmento, Synthesis and characterization of chitosan-grafted-polycaprolactone micelles for modulate intestinal paclitaxel delivery, Drug Deliv. Transl. Res., 8 (2018) 387-397.
[25] S.M. Martins, T. Wendling, V.M. Gonçalves, B. Sarmento, D.C. Ferreira, Development and validation of a simple reversed-phase HPLC method for the determination of camptothecin in animal organs following administration in solid lipid nanoparticles, J. Chromatogr. B, 880 (2012) 100-107.
[26] R. Schellekens, F. Stuurman, F. Van der Weert, J. Kosterink, H. Frijlink, A novel dissolution method relevant to intestinal release behaviour and its application in the evaluation of modified release mesalazine products, Eur. J. Pharm. Sci., 30 (2007) 15-20.
[27] T. Higuchi, Mechanism of sustained-action medication. Theoretical analysis of rate of release of solid drugs dispersed in solid matrices, J. Pharm. Sci., 52 (1963) 1145-1149.
[28] R.W. Korsmeyer, R. Gurny, E. Doelker, P. Buri, N.A. Peppas, Mechanisms of solute release from porous hydrophilic polymers, Int. J. Pharm., 15 (1983) 25-35.
[29] P.L. Ritger, N.A. Peppas, A simple equation for description of solute release II. Fickian and anomalous release from swellable devices, J. Control. Release, 5 (1987) 37-42.
[30] M.H. Macedo, A.S. Barros, E. Martínez, C.C. Barrias, B. Sarmento, All Layers Matter: Innovative Three-dimensional Epithelium-Stroma-Endothelium Intestinal Model for Reliable Permeability Outcomes, Submitted, (2021).

716 [31] M.H. Macedo, E. Martinez, C.C. Barrias, B. Sarmento, Development of an
717 improved 3D in vitro intestinal model to perform permeability studies of
718 paracellular compounds, Front. Bioeng. Biotechnol. , 8 (2020) 1076.
719 [32] J.P. Rao, K.E. Geckeler, Polymer nanoparticles: preparation techniques and
720 size-control parameters, Prog. Polym. Sci., 36 (2011) 887-913.
721 [33] J.W. Hickey, J.L. Santos, J.-M. Williford, H.-Q. Mao, Control of polymeric
722 nanoparticle size to improve therapeutic delivery, J. Control. Release, 219 (2015)
723 536-547.
724 [34] H. Yuan, L.-J. Lu, Y.-Z. Du, F.-Q. Hu, Stearic acid-g-chitosan polymeric
725 micelle for oral drug delivery: in vitro transport and in vivo absorption, Mol.
726 Pharm., 8 (2011) 225-238.
727 [35] D.S. Silva, A. Almeida, F.G. Prezotti, W.M. Facchinatto, L.A. Colnago, S.P.
728 Campana-Filho, B. Sarmento, Self-aggregates of 3, 6-O, O'-dimyristoylchitosan
729 derivative are effective in enhancing the solubility and intestinal permeability of
730 camptothecin, Carbohydr. Polym., 177 (2017) 178-186.
731 [36] L. Tu, G. Wang, N. Qi, W. Wu, W. Zhang, J. Feng, Multi-functional chitosan
732 polymeric micelles as oral paclitaxel delivery systems for enhanced bioavailability
733 and anti-tumor efficacy, International journal of pharmaceutics, 578 (2020)
734 119105.
735 [37] L. Li, N. Liang, D. Wang, P. Yan, Y. Kawashima, F. Cui, S. Sun, Amphiphilic
736 polymeric micelles based on deoxycholic acid and folic acid modified chitosan for
737 the delivery of paclitaxel, Int. J. Mol. Sci., 19 (2018) 3132.
738 [38] ISO/EN10993-5. International Standard ISO 10993-5 Biological Evaluation
739 of Medical Devices—Part 5: Tests for Cytotoxicity: In Vitro Methods, in,
740 International Organization for Standardization, Geneva, Switzerland, 2009.
741 [39] P. Laskar, S. Samanta, S.K. Ghosh, J. Dey, In vitro evaluation of pH-sensitive
742 cholesterol-containing stable polymeric micelles for delivery of camptothecin, J.
743 Colloid Interface Sci., 430 (2014) 305-314.
744 [40] P. Luo, Y. Luo, J. Huang, W. Lu, D. Luo, J. Yu, S. Liu, Incorporation of
745 camptothecin into reduction-degradable supramolecular micelles for enhancing
746 its stability, Colloids Surf. B, 109 (2013) 167-175.
747 [41] Y. Du, L. Ling, M. Ismail, W. He, Q. Xia, W. Zhou, C. Yao, X. Li, Redox
748 sensitive lipid-camptothecin conjugate encapsulated solid lipid nanoparticles for
749 oral delivery, Int. J. Pharm., 549 (2018) 352-362.

[42] T.-H. Yeh, L.-W. Hsu, M.T. Tseng, P.-L. Lee, K. Sonjae, Y.-C. Ho, H.-W. Sung, Mechanism and consequence of chitosan-mediated reversible epithelial tight junction opening, Biomaterials, 32 (2011) 6164-6173.

[43] R. Mo, X. Jin, N. Li, C. Ju, M. Sun, C. Zhang, Q. Ping, The mechanism of enhancement on oral absorption of paclitaxel by N-octyl-O-sulfate chitosan micelles, Biomaterials, 32 (2011) 4609-4620.

[44] H. Yuan, L.-J. Lu, Y.-Z. Du, F.-Q. Hu, Stearic acid-g-chitosan polymeric micelle for oral drug delivery: in vitro transport and in vivo absorption, Molecular pharmaceutics, 8 (2011) 225-238.

[45] A. Narai, S. Arai, M. Shimizu, Rapid decrease in transepithelial electrical resistance of human intestinal Caco-2 cell monolayers by cytotoxic membrane perturbents, Toxicol. In Vitro, 11 (1997) 347-354.

[46] I. Behrens, T. Kissel, Do cell culture conditions influence the carrier-mediated transport of peptides in Caco-2 cell monolayers?, Eur. J. Pharm. Sci., 19 (2003) 433-442.

[47] A.H. Fischer, K.A. Jacobson, J. Rose, R. Zeller, Hematoxylin and eosin staining of tissue and cell sections, CSH Protoc., (2008).

[48] T. Woraphatphadung, W. Sajomsang, P. Gonil, A. Treetong, P. Akkaramongkolporn, T. Ngawhirunpat, P. Opanasopit, pH-Responsive polymeric micelles based on amphiphilic chitosan derivatives: Effect of hydrophobic cores on oral meloxicam delivery, Int. J. Pharm., 497 (2016) 150-160.

[49] P. Dramou, M. Fizir, A. Taleb, A. Itatahine, N.S. Dahiru, Y.A. Mehdi, L. Wei, J. Zhang, H. He, Folic acid-conjugated chitosan oligosaccharide-magnetic halloysite nanotubes as a delivery system for camptothecin, Carbohydr. Polym., 197 (2018) 117-127.

[50] Y. Du, L. Ling, M. Ismail, W. He, Q. Xia, W. Zhou, C. Yao, X. Li, Redox sensitive lipid-camptothecin conjugate encapsulated solid lipid nanoparticles for oral delivery, International journal of pharmaceutics, 549 (2018) 352-362.